Earth and Planetary Science Letters 274 (2008) 301–309

Contents lists available at ScienceDirect

Earth and Planetary Science Letters

journal homepage: www.elsevier.com/locate/epsl

Convective interactions between oceanic lithosphere and asthenosphere: Influence of a transform fault

C. Dumoulin [a,b,*], G. Choblet [a,b], M.P. Doin [c]

[a] Université Nantes Atlantique, Laboratoire de Planétologie et Géodynamique de Nantes, 2 rue de la Houssinière, 44322 Nantes cedex 03, France
[b] CNRS, UMR-6112, 2 rue de la Houssinière, 44322 Nantes cedex 03, France
[c] CNRS, UMR-8536, Ecole Normale Supérieure de Paris, 24 rue Lhomond, Paris, F-75005, France

ARTICLE INFO

Article history:
Received 23 January 2008
Received in revised form 7 July 2008
Accepted 10 July 2008
Available online 20 July 2008

Editor: C.P. Jaupart

Keywords:
oceanic lithosphere
transform fault
small-scale convection

ABSTRACT

Current estimates of the asthenospheric viscosity favor the occurrence of small-scale convection (SSC) beneath oceanic lithosphere of sufficient age. Since transform faults (TFs) juxtapose lithospheres of distinct ages (and thicknesses), they are likely to influence their dynamics. In this paper, we describe 3D numerical models of oceanic spreading for two ridge segments offset by a TF in domains that are sufficiently large for SSC to fully develop. A framework based on thermal convection with temperature-dependent viscosity and both internal and basal heating is adopted and parameters such as surface velocity, age offset at the TF, activation energy, mantle viscosity, and internal heating rate are explored. In our numerical experiments, the onset time for SSC is identical on each side of the fracture zone (FZ). It is not modified by the presence of a TF. Moreover, scaling relationships for the onset time obtained in 2D experiments remain valid. Earlier studies focused on the influence of a TF based on 2D experiments corresponding to slices parallel to the ridge axis. They noted the rapid development of a sinking thermal instability located at the step in the lithospheric relief. Our results indicate that the wake of the TF is characterized by the development of a lateral, "edge-driven", buoyant flow, from the younger (thinner) side to the older (thicker) side of the FZ. However, due to the global shearing context, this instability does not sink before the onset of SSC (characterized by small-scale instabilities on each side of the FZ, as observed in earlier studies). The essentially 3D velocity field, combining this lateral flow and the prescribed surface spreading velocity, results in an angle formed by the TF trail with the spreading direction. We describe the parameters controlling this angle in our experiments and propose a scaling relationship. In oceanic settings, the specific geometry of the ridge axis (segment length, orientation of the TFs) may affect this angle. In addition, a large scale mantle flow of other geodynamical origin could interact with the spreading flow, and also modify the TF trail angle. This departure at depth of the boundary between the thick and thin lithospheres from the surface FZ may explain the presence of oceanic volcanoes on the older side of the FZ (usually considered as thicker).

1. Introduction

Though the oceanic lithosphere plays a major role in the Earth's cooling history, the dynamics of this shallow structure is as controversial a topic as the deeper nature of global mantle convection. Its thermal structure has first been described as simply resulting from cooling in a purely conductive half-space (Turcotte and Oxburgh, 1967). However, several features of old oceanic lithosphere cannot be explained by this simple model: the flattening of ocean floor bathymetry (Parsons and Sclater, 1977), geoid anomalies in the Center Pacific Ocean and in the South Indian Ocean (Haxby and Weissel, 1986), gravity amplitude and wavelength observed for large areas of the same oceans (Buck and Parmentier, 1986), as well as seismic velocity models from surface wave dispersion indicating that the Pacific plate may experience a reheating process at ages greater than 70 Myr (Ritzwoller et al., 2004), for example. Since then, a long-standing debate exists on the origin and precise amount of the departure of bathymetry and surface heat flow with age from the evolution predicted by the Half-Space cooling model (Maggi et al., 2006; Crosby et al., 2006; Zhong et al., 2007).

One important group of studies have interpreted this departure as an indication of the presence of small-scale convection (SSC) (Parsons and McKenzie, 1978; Davaille and Jaupart, 1994; Doin and Fleitout, 2000). More sophisticated conductive models have thus been established in order to take into account the heat flux provided by SSC at the base of the lithosphere. The Plate model (Parsons and Sclater, 1977; Stein and Stein, 1992), and the Chablis model (Doin and

* Corresponding author. Université Nantes Atlantique, Laboratoire de Planétologie et Géodynamique de Nantes, 2 rue de la Houssinière, 44322 Nantes cedex 03, France. Tel.: +33 2 51 12 54 80; fax: +33 2 51 12 52 68.
E-mail address: caroline.dumoulin@univ-nantes.fr (C. Dumoulin).

0012-821X/$ – see front matter © 2008 Elsevier B.V. All rights reserved.
doi:10.1016/j.epsl.2008.07.017

Fleitout, 1996; Dumoulin et al., 2001) use different boundary conditions to describe this basal heating. Many studies derived scaling relationships of the onset time of SSC using, in most cases, the assumption that onset occurs when the boundary layer reaches its marginal stability state, i.e. some locally defined Rayleigh number reaches a critical value. However, the definition of this local Rayleigh number differs from one study to another, as well as the settings of experiments (laboratory or numerical with 2D or 3D cartesian geometry, range of viscosity temperature-dependence, for example) (Davaille and Jaupart, 1994; Marquart et al., 1999; Huang et al., 2003; Korenaga and Jordan, 2003; Zaranek and Parmentier, 2004; Dumoulin et al., 2005). These scalings can then be used to provide estimates on the minimum age of the lithosphere whose thermal structure is modified by SSC and the amplitude of the basal heat flux.

The goal of the present study is not to explore the question of whether the origin of the possible flattening of seafloor depth with age should be attributed to SSC or to competing explanations such as asthenospheric flow (Phipps Morgan and Smith, 1992), impinging plumes (Crough, 1978), dynamic topography (Cazenave and Lago, 1991), or radiogenic heating (Huang and Zhong, 2005) or to a combination of these mechanisms. We consider here the fact that the viscosity at the base of the lithosphere is sufficiently low for thermal instabilities to develop at ages smaller than 150 Myr (i.e. $\sim 10^{18}$–10^{19} Pa s, see Dumoulin et al., 2005). Apart from the large scale effect on bathymetry and heat flow, the dynamics of such instabilities are also likely to be relevant for the analysis of small scale topography or gravimetry anomalies of the ocean floor, and of the seismic anisotropic pattern (Montagner, 2002). Several studies also showed that SSC may be responsible for intraplate volcanism that cannot be associated to hotspots (Haxby and Weissel, 1986; Doin and Fleitout, 1996; Raddick et al., 2002; Ballmer et al., 2007). Richter and Parsons (1975) demonstrated that SSC under large-scale shearing is reorganized as rolls perpendicular to the ridge. Dynamics of lithosphere–asthenosphere interaction under a moving plate has been numerically studied in 2-D simulations (Dumoulin et al., 2001; Huang and Zhong, 2005) (thus with SSC rolls parallel to the ridge axis), as well as with 3-D cartesian geometry (Marquart, 2001; van Hunen et al., 2003; Morency et al., 2005).

More precisely, our aim is to assess the influence of a transform fault (TF) off-setting two ridge segments on SSC dynamics. The ridge/transform system, has been the subject of seminal studies where a steady-state 3D passive flow and the resulting melt production were considered (Phipps Morgan and Forsyth, 1988; and with a more realistic rheology, Shen and Forsyth, 1992): these results were also considered in terms of their gravitational implications (Blackman and Forsyth, 1991). However, these studies focused mainly on the ridge axis so that the region considered in the model does not extend up to the ages where lithospheric instabilities might occur. More recently, 2D numerical studies (Sleep, 2002; Huang et al., 2003; Dumoulin et al., 2005) have shown that the large horizontal thermal gradient created by a TF induces instabilities at very small ages compared to the initiation of SSC under an homogeneous oceanic lithosphere. These 2D models mimic a 3D simulation by computing the flow in vertical slices parallel to the ridge axis, considering that the time-evolution of a transient 2D flow is similar to a steady-state 3D flow away from the ridge axis. Therefore, the 2D models lack the dynamics resulting from the coupling of the velocity component in the direction perpendicular to the ridge axis with the flow components within the 2D planes parallel to the ridge. In a 3D model with an oblique ridge axis displaying several segments offset by transforms, Morency et al. (2005) demonstrated that the rolls resulting from the SSC instabilities develop in a direction oblique to the spreading velocity. Although some of this numerical experiments considered several ridge segments offset by transforms, the goal of this study was rather to assess the influence of the large scale geometry of the ridge axis on the resulting SSC than to study specifically the local consequences of a transform fault on the flow.

Here, we further investigate this 3D flow geometry by looking at the effect of a single TF on the lithospheric structure and underlying flow. We first present briefly the numerical method and physical model (Section 2). We then describe the flow obtained with numerical experiments using various parameter values (Section 3). In the two following parts, we analyze the onset times of SSC and compare our results to previous scaling laws (Section 4), and describe a specific permanent feature observed in all our experiments, the "transform fault trail", systematically oriented towards the older lithosphere (Section 5). Finally, we discuss the possible implications of our simple models on the surface observables (Section 6).

Table 1
Characteristic scales and parameters values

Symbol	Description	Value/unit
d	Thickness of the layer	670 km
ΔT	Global temperature difference	1800–273 = 1527 K
k	Thermal conductivity	3.1 W m^{-1} K^{-1}
κ	Thermal diffusivity	8×10^{-7} m^2 s^{-1}
α	Thermal expansion coefficient	3.5×10^{-5}K^{-1}
ρ_0	Mantle reference density	3300 kg m^{-3}
R	Gas constant	8.31 J mol^{-1}K^{-1}
g	Gravitational acceleration	9.81 m s^{-2}

Table 2
List of the numerical experiments

n°	V_s (cm yr^{-1})	Δt_{TF} (Myr)	E_a (kJ mol^{-1})	Ra –	τ_{old} (Myr)	τ_{young} (Myr)	θ (°)
1	0.56	37	176	5×10^7	37.1	40.8	19.17
2	1.13	18	264	3×10^7	74.1	72.3	9.51
3	1.88	11	176	10^7	85.6	76.7	4.84
4	1.88	11	212	3×10^7	44.5	50.1	6.80
5	1.88	45	212	3×10^7	51.2	50.1	9.96
6	1.88	11	176	5×10^7	25.6	25.6	8.95
7[a]	1.88	11	176	5×10^7	42.3	42.3	9.00
8	1.88	22	176	5×10^7	24.5	26.7	9.60
9	2.82	7	176	5×10^7	24.5	25.2	6.37
10	3.77	5.5	212	8.95×10^7	22.8	23.4	4.79
11	5.65	4	212	1.64×10^8	15.6	15.2	3.76

[a] Simulation with an internal heating rate twice larger than in other simulations.

2. Model setup

We solve the following nondimensional equations for the conservation of mass (Eq. (1)), momentum (Eq. (2)), and energy (Eq. (3)) for an infinite Prandtl number fluid in the Boussinesq approximation:

$$\nabla \cdot \mathbf{u} = 0, \tag{1}$$

$$-\nabla P + \nabla \cdot \left[\nu\left(\nabla \mathbf{u} + \nabla^T \mathbf{u}\right)\right] - Ra T \mathbf{e}_z = 0, \tag{2}$$

$$\frac{\partial T}{\partial t} + \mathbf{u} \cdot \nabla T = \nabla^2 T + H, \tag{3}$$

where $\mathbf{u}$, P, ν, T, and H are velocity, pressure, viscosity, temperature, and volumetric heating, respectively. $\mathbf{e_z}$ is the vertical (positive downside) unit vector. The Rayleigh number, Ra, is defined in the usual way for bottom-heated experiments:

$$Ra = \frac{\alpha \rho_0 g \Delta T d^3}{\kappa \nu_b}. \tag{4}$$

The classical characteristic scales are used: ΔT the temperature across the layer, d the layer thickness, d^2/κ the diffusive timescale, and ν_b the bottom viscosity. Other symbols are defined in Table 1.

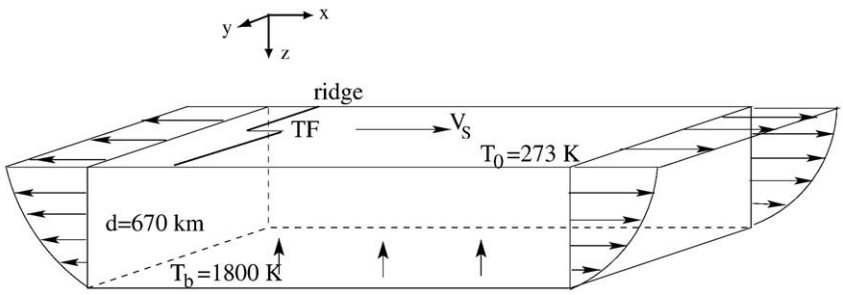

Fig. 1. Boundary conditions and model setup.

The finite difference program used in this study is the 3-D cartesian convection program described in Choblet and Parmentier (2001), with a different transport scheme: advection is treated with an explicit Godunov high resolution scheme. The flow is calculated with a multigrid solver. The mesh contains 128×64×64 grid cells in the xyz directions (for all calculations except case 2, where 128×64×128 grid cells are used, due to larger viscosity contrasts, cf. Table 2), and its aspect ratio is of 4×2×1 (see Fig. 1). An accuracy test has been performed for case 8, with a grid refined in the vertical direction (128×64×128): a comparison with results obtained on a 128×64×64 grid yields an error estimate of 0.98% for the mean surface Nusselt number, and of 0.05% for the mean temperature.

We model the cooling of an oceanic lithosphere from a ridge axis divided in two segments by a transform fault. The mid-ocean ridge spreading geometry is prescribed at the surface by imposing velocities (see Fig. 1). The half spreading rates, V_s, range from 0.5 to 5.65 cm yr^{-1} depending on the calculations (cf. Table 2). The length of the transform fault varies between 210 and 840 km, depending on the calculation, and corresponds to an offset in age (denoted Δt_{TF}) ranging between 4 and 45 Myr (see Table 2). A shear flow in the x-direction, characterized by a constant shear stress τ_{xy}, is prescribed on the left and right (constant x) boundaries. This outgoing flow is counterbalanced by material entering the bottom of the box. A free-slip condition is imposed on the front and back boundaries (constant y), as well as on the bottom boundary for the

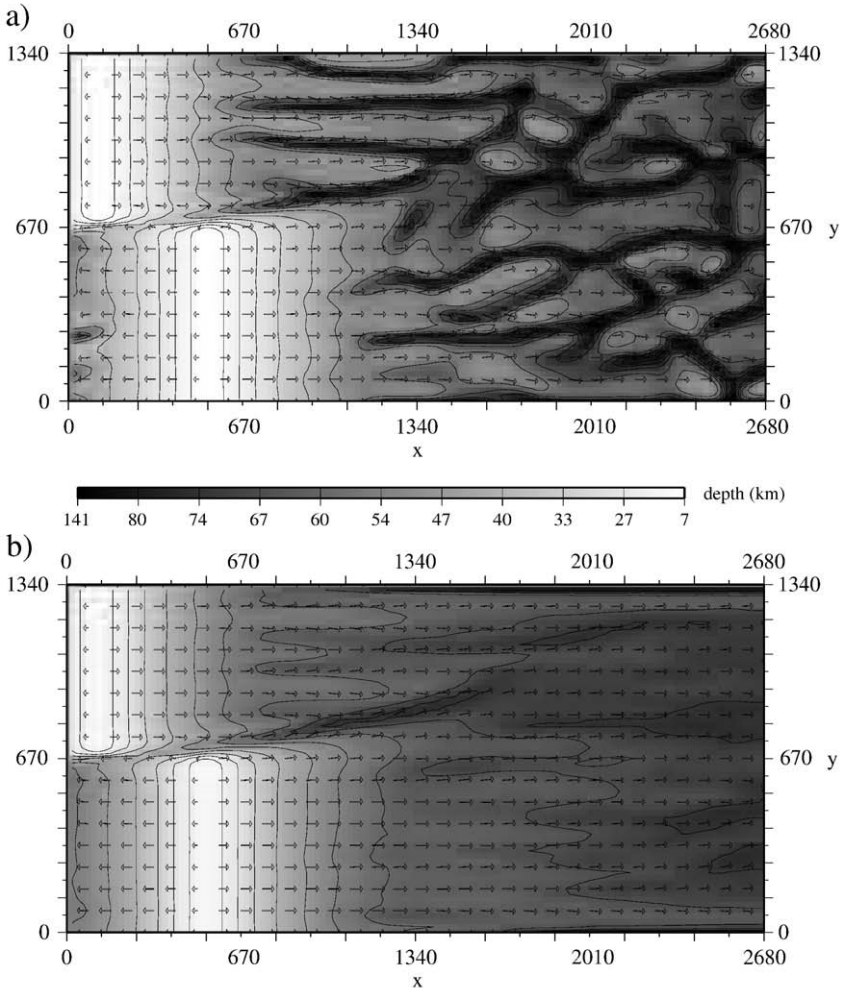

Fig. 2. Lithospheric thickness and flow. Depth of the isotherm corresponding to the base of the lithosphere (gray shade) and horizontal velocity field at this depth (arrows) a) at a given calculation time, and b) averaged in time, for case 8 (described in Table 2). Lengths are in kilometers. Isocontours are drawn every 6.7 km.

horizontal flow. The incoming bottom flow has a constant temperature, T_b, of 1800K, whereas the surface temperature, T_0, is fixed at 273K. In addition to this bottom heating, the box is heated from within using a heat production of 12×10^{-12} W kg^{-1} (for all experiments except case 7, see Table 2) or 25×10^{-12} W kg^{-1} (for case 7). The initial temperature field is the prediction of the half-space cooling model, with a random perturbation of $\pm10^{-3}\Delta T$ added over the whole box.

We use a Newtonian rheology with a temperature-dependent viscosity, using the Frank–Kamenetskii approximation: $\nu = \nu_0 \exp\left(-b\frac{T-T_0}{\Delta T}\right)$, where ν_0 is the reference dynamic viscosity (at the surface). In the framework of this approximation, the coefficient b can be expressed as $b = \frac{E_a \Delta T}{RT_i^2}$, E_a being the activation energy (ranging from 176 to 264 kJ mol^{-1}, depending on calculations, see Table 2), R the gas constant, and T_i the internal temperature. Note that, due to the open bottom boundary condition and internal heating, T_i differs only slightly from the bottom temperature (less than 4%). The bottom viscosity is then $\nu_b = \nu_0 \exp\left(-\frac{Ea\Delta T}{RT_i^2}\right)$. Varying the Rayleigh number leads to variations in ν_0, the reference viscosity, and therefore ν_b. We use here a range of Rayleigh numbers from 10^7 to 1.64×10^8 (see Table 2), corresponding to ν_b ranging between 6.5×10^{19} and 4.0×10^{18} Pa s., in order to study the parameterization of SSC onset times. Each simulation involves two calculation steps: a quasi-static equilibrium is reached in the first step (i.e. when the variables of convection averaged over the whole box oscillate around a constant value), and the second step is used for the analysis of lithospheric dynamics.

3. Flow description

Due to surface boundary conditions, the upper boundary layer thickens when it moves away from the ridge. In the following, the cold boundary layer will be termed lithosphere, in analogy to the Earth. We thus define the base of the lithosphere with an isotherm. The isotherm $T=T_i-\delta T_{eff}/2$ is chosen, with δT_{eff} the temperature difference across the unstable part of the thermal boundary layer. δT_{eff} is proportional to the viscous temperature scale: $\delta T_{eff} = 2.23\left(\frac{Ea\Delta T}{RT_i^2}\right)^{-1}$ (Morris and Canright, 1984; Davaille and Jaupart, 1993). At the onset of small scale convection, dripping thermal instabilities are observed at the base of the lithosphere, on each side of the transform zone (see Fig. 2a for an example). Note that, in Fig. 2a, SSC onset occurs on the older side of the fracture zone (FZ), at a distance of the ridge similar to the TF length. This is a coincidence, and is not seen in most of our simulations (compare, in Table 2, onset times on older side of the FZ, denoted τ_{old}, and age offsets, Δt_{TF}). The position of SSC instabilities is time-dependent. On both sides of the FZ, instabilities occur at the same distance from the ridge axis (see Section 4 for a precise determination and parameterization of the onset time). Instabilities create SSC rolls perpendicular to the ridge axis that deflect the lithospheric isotherms (see Fig. 2a). These features, first described by Richter and Parsons (1975), are now a classical result reproduced in 3D numerical models (van Hunen et al., 2003; Morency et al., 2005). Note that, as the lithosphere grows old, SSC rolls reorganize (coalescences, separations). Fig. 2b displays a time averaged temperature field. Due to

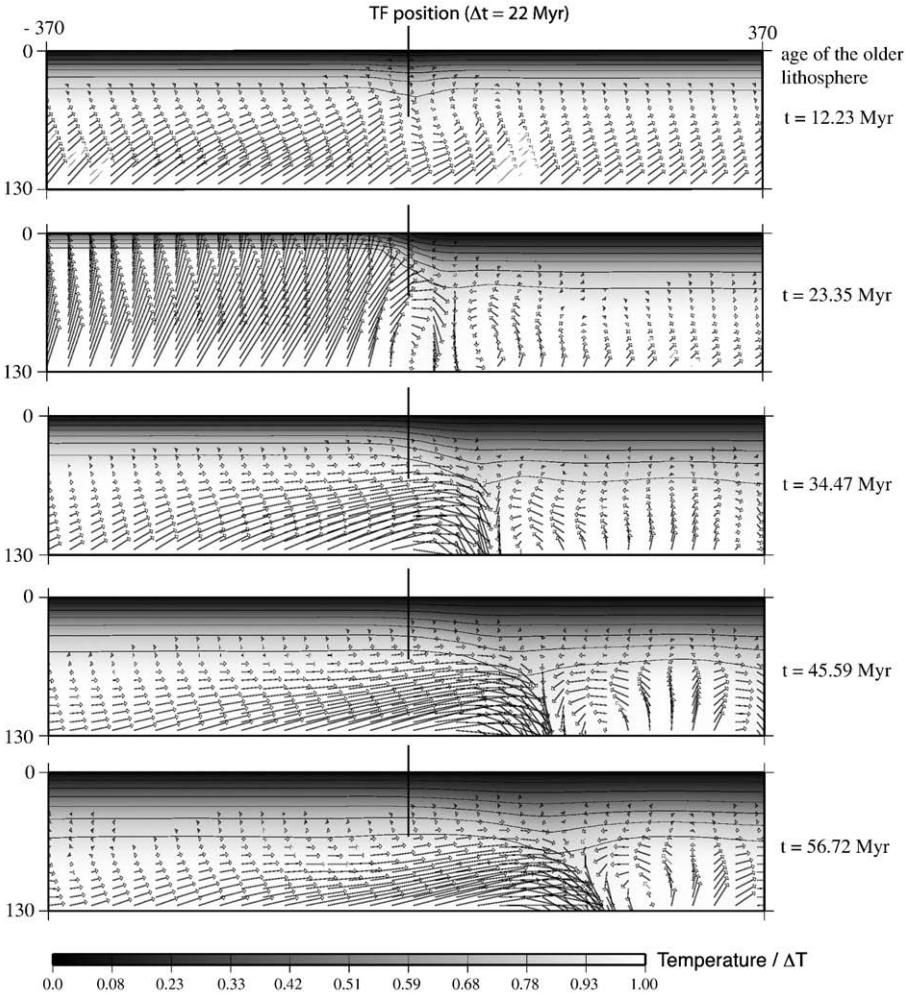

Fig. 3. Vertical (y, z) slices of the averaged temperature field (case 8, see Fig. 2b), zoomed on the FZ location for different x positions (i.e. lithospheric ages). Time-averaged flow velocities are shown with arrows. Lengths are in kilometers. For this case, the two lithospheres have the same thickness at an age of 11 Myr.

the time variability of the locations of the sinking thermal instabilities, the topography of the isotherm is smoothed. Note however that the persistence of small deflections in the average map indicates that thermal instabilities tend to form preferentially at these locations. The averaging stage is based on simulation durations larger than at least the time needed for a particle initially located at the ridge axis to exit the numerical domain through the farthest side of the box. Therefore, these persisting structures are not due to a too small averaging time.

The transform fault induces the coexistence of two lithospheres of different thicknesses: the larger the age offset, the larger the step in the lithospheric structure. The transform fault yields finite horizontal temperature gradients in the thermal boundary layer. In all calculations, a flow in the y direction (from the younger side towards the older side of the FZ) is induced by this step-like increase of the cold boundary layer thickness (see Fig. 3). In the shearing context of our experiments, it is similar to the edge-driven convection model proposed to explain volcanic features near the transition between an oceanic and a continental plate (King and Anderson, 1998). A consequence of this edge-driven flow is the thermal erosion of the step. In all calculations, we observe that, when the lithosphere moves away from the ridge, the step in the lithospheric structure (i.e. the transition between thin and thick lithospheres) deviates towards the older side of the FZ, forming a trail (called TF trail in the following part of the paper). Consequently, the topography of the base of the lithosphere induced by the TF deviates at depth from the surface FZ (see Fig. 2b for an example). Once SSC affects the lithosphere on both sides of the FZ, the TF trail disappears due to the homogenisation of the lithospheric thickness (see Fig. 2b).

A difference between these 3D results and the 2D transient cooling simulations (parallel to the ridge) with a transform fault by Huang et al. (2003) and Dumoulin et al. (2005) lies in the fact that material is here allowed to flow in the x-direction along the TF trail, whereas in 2D simulations it was forced to form sinking thermal instabilities. We note that, on the time-averaged temperature field, the TF trail is the most apparent feature in the lithospheric structure (see Fig. 2b). This implies that the flow induced by the transform fault is persistent, whereas the locations of thermal instabilities on each side of the TF trail vary with time. Indeed, although vertical downgoing velocities are present below the TF trail, there is no temporal variability in the depth of the isotherm of the base of the lithosphere. Note that the chosen range of Rayleigh number is similar to the one leading to a sinking instability located at the step in lithospheric thickness in 2D models (Huang et al., 2003; Dumoulin et al., 2005): thus, the TF trail phenomenon described above should not be attributed to a less vigourous dynamical regime. We will study with more details the angle formed by the TF trail with the FZ in Section 5.

4. Onset of small-scale convection

The onset time of small-scale convection (τ) in 2D or 3D transient experiments has been widely studied. Various parameterizations have been established as functions of mantle properties, depending on the mechanism considered to be responsible of the growth of thermal instabilities (Davaille and Jaupart, 1994; Choblet and Sotin, 2000; Huang et al., 2003; Korenaga and Jordan, 2003; Zaranek and Parmentier, 2004; Dumoulin et al., 2005). Dumoulin et al. (2005) show that two different parameterizations for the onset times provide similar good fits to the computational results: one is based on the assumption that thermal instabilities occur when the lithosphere reaches its marginal stability thickness (Eq. (5)), the other considers that the growth rate of the instabilities controls the development of SSC (Eq. (6)).

$$\tau \simeq 14 Ra_i^{-2/3} \left(\frac{E_a \Delta T}{R T_i^2} \right)^{7/6} \frac{d^2}{\kappa} \tag{5}$$

$$\tau \simeq 31 Ra_i^{-2/3} \left(\frac{E_a \Delta T}{R T_i^2} \right)^{5/6} \frac{d^2}{\kappa} \tag{6}$$

where Ra_i is the internal Rayleigh number, calculated with the internal temperature and its associated viscosity. Note that, in both equations, the dimentionalized onset time does not depend on the chosen box height, d (fixed at 670 km in this study). These two scaling

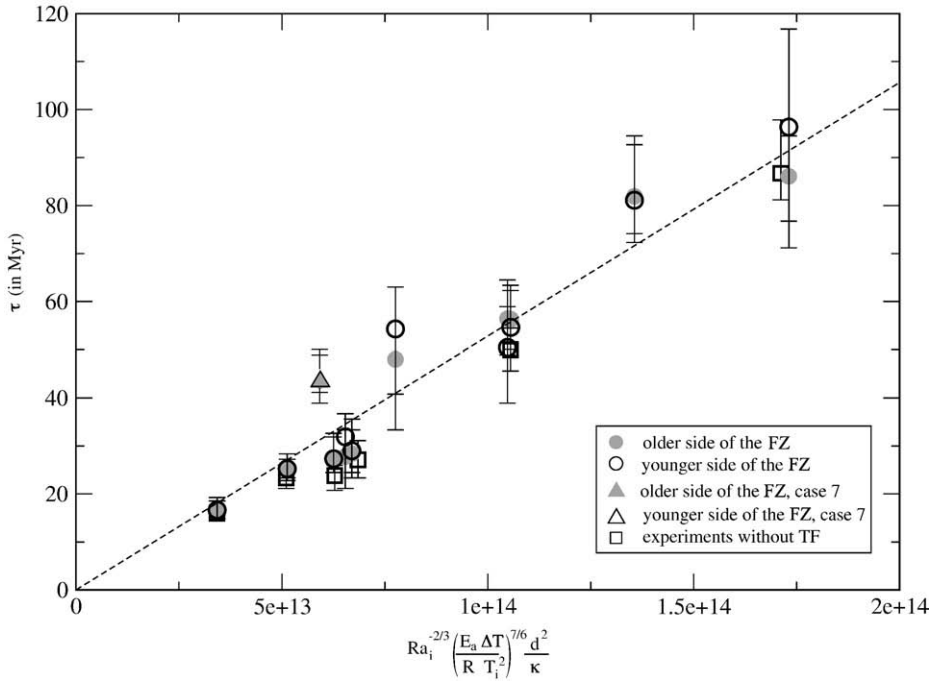

Fig. 4. Time-averaged age of the first thermal instability, τ, as a function of $Ra_i^{-2/3}\left(\frac{E_a \Delta T}{R T_i^2}\right)^{7/6}\frac{d^2}{\kappa}$. Error bars indicate the minimum and maximum ages for a given numerical experiment. A linear regression (dashed line) yields a slope of 16.7 (using onset times in s). Linear correlation coefficient is of 0.96. In case 7, a twice larger heating rate is used.

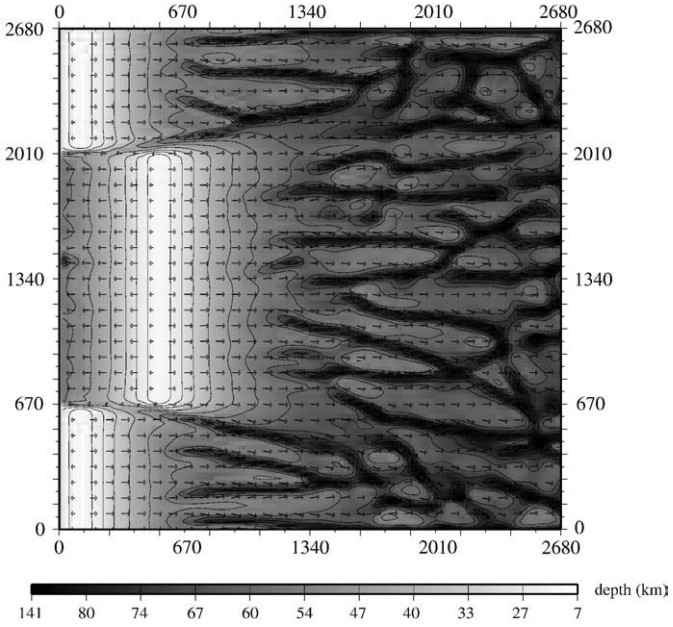

Fig. 5. Depth of the isotherm corresponding to the base of the lithosphere. This case is similar to case 8, but with a box twice wider and two FTs with opposite age offsets.

relationships are consistent with scaling laws proposed by Huang et al. (2003), and Korenaga and Jordan (2003). In 2D transient cooling simulations on a vertical plane parallel to a ridge axis with a transform fault, Huang et al. (2003) and Dumoulin et al. (2005) observed that small-scale convection is triggered at the lithospheric step much sooner than on the sides. However, away from the transform fault, thermal instabilities appear at a time similar to the onset times that would be obtained for a flat lithosphere of the same age (Dumoulin et al., 2005). In the 3D experiments presented here, the flow at the fracture zone cannot be described by the sinking of "drips" but by a permanent shearing of cold lithospheric material along the flow, resulting into an oblique TF trail (Fig. 2b). We therefore only describe onset times of small-scale convection away from the lithospheric step.

In order to estimate the onset times, we first average in time the depth of the isotherm defining the base of the lithosphere (see Fig. 2b for example). We then compute the deviation with time of the depth of the same isotherm with respect to its temporal average. At a given time, the SSC onset is defined as the first deviation (the closest to the ridge) that reaches a given threshold. In the following, we refer to the time average of these values for a given simulation as the SSC onset time. Again, the onset determination is based on sufficiently long simulation durations to ensure a good precision on the value of the onset time.

Onset times together with their time variability obtained on both sides of the transform zone (τ_{old} and τ_{young}) are plotted on Fig. 4 using the parameterization given in Eq. (5). Eq. (6) also provides a good fit to the results (the linear regression yields a slope of 37.0, and a correlation coefficient of 0.94). Note that in Eqs. (5) and (6), the internal heating rate is not taken into account. Therefore, case 7 (plotted with triangles) corresponding to an internal heating rate twice larger than the other cases, is located quite far from the regression line. This case is to be compared to case 6, performed with the exact same parameters except for heating rate. When internal heating rate increases, lithospheres thicken more slowly and thus delay the appearance of thermal lithospheric instabilities. Fig. 4 shows that, as for 2D simulations, small-scale convection is triggered on each side of the FZ at the same lithospheric age. In order to verify the lack of influence of the TF on the onset of SSC away from the FZ, we performed some experiments with the same parameters as for cases 3, 4, 6, 9, 10, and 11 (see Table 2), but without a TF. The onset times obtained with these new experiments (square symbols on Fig. 4) are similar to the ones obtained with a TF. Moreover, cases that only differ by their age offset across the TF yield similar SSC onset times (compare case 4 to case 5, and 6 to 8). It is therefore obvious that the presence of transform faults does not induce smaller or larger SSC onset times at the base of the lithosphere. Dumoulin et al. (2005) showed that onset times obtained in 2D experiments perpendicular to the ridge are well described by Eqs. (5) and (6), although these parameterizations have been established for 2D transient cooling studies. Fig. 4 shows that these scaling laws also provide a good fit to 3D experiments of lithospheric cooling with or without a TF.

5. Trail of the transform fault

As described in Section 3, the TF trail is oriented towards the older lithosphere (see Fig. 2). We analyze the influence of imposed boundary conditions and of the flow induced by the lateral variations of the lithospheric thickness (and thus of lateral buoyancy contrasts) on the TF trail geometry. A simulation is performed using parameters of case 8, but with a box twice wider and two TFs with opposite age offsets. As expected, we observe two trails, of the same amplitude and opposite direction in y (see Fig. 5). We also performed a calculation with the same parameters as for case 8 (including box size and ridge geometry) but setting the buoyancy force to zero (Ra=0). Thermal

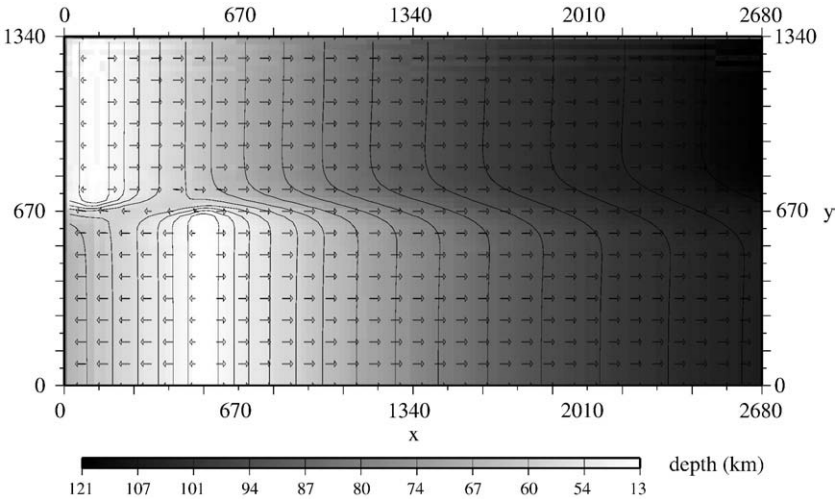

Fig. 6. Depth of the isotherm corresponding to the base of the lithosphere. This case is similar to case 8, but with no buoyancy force (Ra=0).

diffusion and the imposed shearing flow pattern are then the only mechanisms governing the solution. Fig. 6 shows the depth of the base of the lithosphere and should be compared to Fig. 2. Since thermal diffusion smoothes out the lithospheric step in a symmetrical way, there is no deviation towards the older side. From these two tests, we conclude that the deviation of the TF trail observed in our experiments results from the buoyant flow driven by the step in the lithospheric structure.

In order to estimate the angle formed by the TF trail with the direction of the TF, we define at each x the TF trail by the y-position of the maximal depth of the base of the lithosphere on the time averaged temperature field. The angle, θ, is then calculated as described on the lower right corner inset in Fig. 7. Angles obtained for each experiment are listed in Table 2.

We propose that the angle of the TF trail is mainly controlled by the ratio of the buoyancy driven flow and the imposed shear driven flow. The convective flow is assumed to follow a scaling law established for SSC under a stagnant lid and with internal heating (Solomatov and Moresi, 2000). The internal velocity, v_i, due only to SSC buoyancy (approximation that may be valid here in the y direction) can be parameterized as follow (Solomatov and Moresi, 2000):

$$v_i = 0.385\left(Ra_i \frac{RT_i^2}{E_a \Delta T}\right)^{1/2} \frac{\kappa}{d} \tag{7}$$

The shear flow is proportionnal to V_s. On Fig. 7, we show that $\tan(\theta)$ increases with the ratio v_i/V_s.

However, the velocity in the y-direction that deviates the TF trail is, in our simulations, influenced by several parameters that do not appear in Eq. (7). First of all, a larger age offset at the TF enhances the TF trail angle (compare cases 5 and 8 to cases 4 and 6, respectively, cf Fig. 7). This emphasizes the importance of the density contrast across the FZ on the flow control. Another parameter is the internal heating rate, which is larger in case 7 than in other cases. Therefore, case 7 has larger internal velocities due to buoyancy than case 6, but also a slower cooling of the lithosphere, damping the size of the lithospheric step due to TF. These two effects have an opposite role on the angle of the TF trail. Indeed, case 7 exhibits a TF trail angle very close to case 6. Finally, the box size in the y-direction influences the lateral velocity: doubling the size of the box in the direction of the ridge axis (thus doubling the distance between the TF and the boundaries perpendicular to the ridge axis) for case 8 enhances the TF trail angle by 20%. This occurs because the scale of the edge-driven flow that causes the TF trail is controlled by the box dimensions, although it is driven by local buoyancy contrasts. It will therefore be influenced by the experimental setup. Conversely, the small-scale flow that develops when the lithosphere grows old will less be affected by the size of the box. We discuss in the next section the applicability of our scaling to the Earth's oceanic lithosphere.

6. Discussion

6.1. Oceanic lithosphere, SSC and TF trail

"Asthenospheric" viscosities range in our experiments between 4.0×10^{18} and 6.5×10^{19} Pa s. These low values compared to average mantle viscosities derived from post-glacial rebound (Cathles, 1975), are in good agreement with the results of studies including an asthenosphere below the oceanic lithosphere either based on post-glacial rebound (Sigmundsson, 1991; Fjeldskaar, 1994), or on dynamic modeling (Čadek and Fleitout, 1999, 2003). These viscosities allow the development of time-dependent thermal instabilities at the base of the lithosphere, that interact with the imposed large-scale circulation. It may be argued that the relevance of these relatively low asthenospheric viscosities may not extend down to the base of our model. We consider that this does not affect the major findings of this study that are triggered by the local value of viscosity at the base of the lithosphere. Our results predict a permanent lateral flow beneath the FZ that deviates the wake of the transform fault and forms the TF trail angle. In addition to SSC, this feature is likely to exist beneath the oceanic lithosphere. This is a major difference with conclusions of previous 2D transient cooling studies (Sleep, 2002; Huang et al., 2003; Dumoulin et al., 2005), where a sharp topography of the lithosphere (as the one created by a TF for example) induces the birth of time-

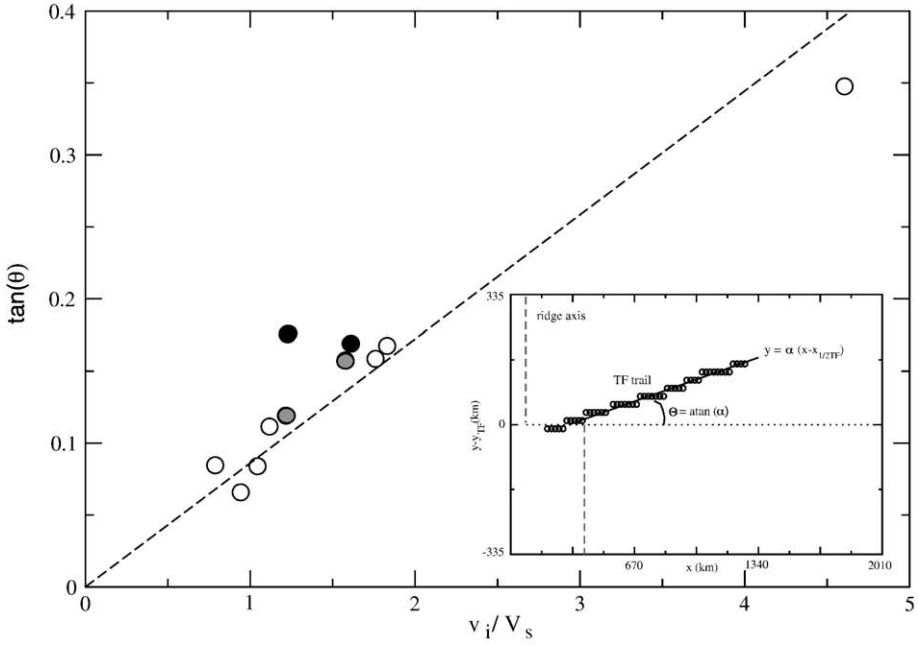

Fig. 7. $\tan(\theta)$ (θ being the angle of the TF trail with the spreading velocity) versus the ratio between buoyancy driven velocity, v_i, and spreading velocity, V_s. The linear regression (dashed line) yields a slope of 0.086, and the correlation coefficient is of 0.95. Black symbols correspond to cases 5 and 8, experiments that use exactly the same parameters as cases 4 and 6, respectively (illustrated with grey circles), but with a larger TF age offset. The lower corner inset displays the TF trail location, in the (x,y) frame, tracked by the deepest locations of the base of the lithosphere, on the time averaged temperature field of case 8.

dependent cold drips sooner than the SSC onset expected for a flat lithosphere. Indeed, the two-dimensional geometry does not allow material to be sheared along the base of the lithosphere but rather force it to sink.

These two alternative patterns (2D or 3D) should lead to different surface observations in terms of volcanic activity, heat flow and gravimetric or topographic measurements across FZs. Hall and Gurnis (2005) showed that a large number of gravity profiles across numerous mature Pacific fracture zones exhibits a signal systematically higher than expected on the older side, at a distance of less than 100 km. Using a viscoelastoplastic model that takes into account both fault friction on FZ and edge-driven convection below the FZ, they conclude that the thermal erosion of the lithospheric step is not strong enough to predict the observed deflections in the gravity profiles. They finally interpret these anomalies as the consequence of moderate extension. However, due to the TF trail migration observed in our 3D simulations, the topography of lithospheric isotherms might differ from their 2D cases and therefore lead to a possible explanation of these gravity anomalies. This should be tested in a subsequent study incorporating a more realistic rheology than the one used here.

Since plate configuration, and thus spreading directions, change on time intervals of some tens of millions of years, it may have impacts on SSC rolls orientation. Van Hunen and Zhong (2006) showed that it takes at least 20 Myr to fully reorganize the SSC axis along the new spreading direction that is oblique to inherited lithospheric structures. However, since SSC onset times are controlled by the local thermal structure due to conductive cooling, they should not be affected by such plate configuration changes. The edge-driven flow is associated to the lithospheric step, and therefore exists independently of these changes. Moreover, the TF trail develops at very young ages, smaller than the characteristic time for plate reorientation.

6.2. Lateral extent of the edge-driven flow

The scaling of the TF trail angle proposed for our experiments (cf. Fig. 5) can be applied to real cases, but the specific geometry of the oceanic ridge segments needs to be taken into account. First, the angle varies slightly with the lateral size of the numerical domain. A smaller size inhibits the “edge-driven” convective flow induced by the lateral density contrast. It can however be expected from our experiments that if the lateral dimension of the domain is large enough, the lateral velocity, and therefore the TF trail angle will reach an asymptotic value. The geometry of our simulations could apply to oceanic areas where only few TFs associated with large age offsets affect a relatively long linear ridge segment (as observed on the East Pacific Rise, for example). On the other hand, in some cases, the lateral flow produced by TF is likely to be bounded laterally by a neighbouring TF of opposite direction (see Fig. 5) or another natural barrier. This occurs between Kane and Atlantis FZs on the Mid-Atlantic Ridge, for example, and on a more local scale between Dutoit (25° E) and Prince Edward (35° E) FZs on the Southwest Indian Ridge, for example.

Another case is when successive TFs displace the ridge axis systematically in the same direction. Morency et al. (2005) showed that such a long sequence of TFs induces at depth a large-scale flow that is oblique to the spreading direction. This feature is observed in anisotropic maps from some tomographic studies of the south Pacific ocean and Indian ocean at young ages (Montagner, 2002; Debayle and Sambridge, 2004), and therefore possibly before the SSC onset. Our simple parameterization of the TF trail angle provides values that are smaller than observed in Morency et al. (2005)'s models. Therefore, a long sequence of TFs should enhance the lateral flow velocity: the addition of several lithospheric steps builds up an increased TF trail angle compared to the single TF case. Regions where such a configuration is observed are quite common both on the Mid-Atlantic Ridge and the various ridges of the Indian Ocean.

6.3. TF trail deviation and volcanoes locations

A consequence of the offset between the lithospheric steps at depth and the surface FZs location may be associated to a paradox noted by Sleep (2002). The oceanic lithosphere might be subjected to the impacts of plumes inducing off-axis volcanoes. The impounded mantle plume material at the base of the lithosphere should follow the lithospheric relief. One thus expects the plume material to cascade from the older (thicker) to the younger (thinner) lithosphere, if lithospheric relief remains below the surface FZs. However, some oceanic volcanic islands (such as the Marquesas group), while relatively close to a FZ, are located on the older side. This phenomenon is explained by Sleep (2002) in the old ocean basins, by the additional heat supplied by SSC to the base of the lithosphere and the disappearance of lithospheric relief beneath the FZ.

We argue here, that, even on young oceanic lithosphere, volcanic features may be observed on the older side of the FZ, due to the TF trail angle at depth. These volcanoes could be attributed either to a plume impact as proposed by Sleep (2002) or to decompression melting due to the upwelling structures associated to the edge-driven flow (see Fig. 3) as described by Ballmer et al. (2007) in the small-scale convection context. This last phenomenon may build a non-age sequential ocean–island chain. Further observations of such volcanoes on the older side of a FZ (but close to it) would confirm the mechanism proposed in this study. They are out of the scope of the present paper.

7. Conclusions

We used 3D numerical simulations of mantle convection to study the oceanic lithosphere associated to two mid-oceanic ridge segments offset by a transform fault (TF). The results are as follows:

(1) The onset of small-scale convection (SSC) occurs at the same age on both the older and younger lithospheres. It is well described by the scaling laws established for 2D transient cooling studies (Dumoulin et al., 2005). Simulations performed without a TF also lead to similar onset times for SSC. These results indicate that the TF does not favor nor delay the initiation of SSC under the oceanic lithosphere.

(2) Below the fracture zone (FZ), a permanent lateral flow is observed whatever the age of the lithosphere, even for ages smaller than SSC onset time. This edge-driven flow, from the younger to the older lithosphere, not observed in earlier 2D transient cooling studies (Sleep, 2002; Huang et al., 2003; Dumoulin et al., 2005), is stationary. Thus, we do not consider this flow as part of SSC.

(3) This permanent flow below the FZ is driven by lateral variations of buoyancy across it. The greater the age offset –and consequently the buoyancy contrast–, the larger the lateral flow velocity. The “asthenospheric” flow below the FZ is then a combination between this buoyant flow (parallel to the ridge axis) and the shear flow associated to spreading (orthogonal to the ridge axis in our experiments). It erodes thermally the lithospheric step and deviates it towards the old lithosphere. Therefore, the deep TF trail does not underlie the surface FZ, even at very young ages. The angle of the TF trail with the surface FZ scales correctly with the ratio of the internal velocity due to buoyancy over the spreading velocity. When SSC becomes well developed at least on the older side of the FZ, the TF trail vanishes.

(4) Since the TF trail deviation is obtained in our numerical experiments for a plausible range of mantle viscosity, it should be expected for oceanic lithosphere. A succession of TFs displacing the ridge axis in the same direction may tend to build up a lateral flow of larger amplitude than the one predicted in this study for a single TF. On the contrary, adjacent

TFs with opposite age offsets may decrease the lateral flow. In any case, measuring the TF trail angle for various TFs should constrain the amplitude of buoyancy driven flow in the uppermost mantle beneath the oceanic lithosphere.

(5) Finally, the deviation at depth of the boundary between the young and old lithosphere provides a good explanation for the paradoxical presence of volcanoes close to FZ but on its older (and therefore usually assumed as thicker) side of the FZ. These magmatic features could either be associated to hot plumes of deeper origin or to decompression melting induced by the edge-driven flow.

Acknowledgements

We thank L. Elkins-Tanton and an anonymous reviewer for their very constructive remarks helping to improve the clarity of the manuscript. This work has benefited from a grant from CNRS/INSU DyETI program and calculations have been performed on the CINES's supercomputer.

References

Ballmer, M.D., van Hunen, J., Ito, G., Tackley, P.J., Bianco, T.A., 2007. Non-hotspot volcano chains originating from small-scale sublithospheric convection. Geophys. Res. Lett. 34. doi:10.1029/2007GL031636.

Blackman, D.K., Forsyth, D.W., 1991. Isostatic compensation of tectonic features of the Mid-Atlantic Ridge: 25°–27°30′S. J. Geophys. Res. 96, 11741–11758.

Buck, W.R., Parmentier, E.M., 1986. Convection beneath young oceanic lithosphere: implications for thermal structure and gravity. J. Geophys. Res. 91, 1961–1974.

Čadek, O., Fleitout, L., 1999. A global geoid model with imposed plate velocities and partial layering. J. Geophys. Res. 104, 29055–29075.

Čadek, O., Fleitout, L., 2003. Effect of lateral viscosity variations in the top 300 km on the geoid and dynamical topography. Geophys. J. Int. 152, 566–580.

Cathles, L.M., 1975. The viscosity of the Earth's mantle. Princeton University Press, Princeton, NJ.

Cazenave, A., Lago, B., 1991. Long wavelength topography, sea-floor subsidence and flattening. Geophys. Res. Lett. 18, 1257–1260.

Choblet, G., Parmentier, E.M., 2001. Mantle upwelling and melting beneath slow spreading centers: effects of variable rheology and melt productivity. Earth Planet. Sci. Lett. 184, 589–604.

Choblet, G., Sotin, C., 2000. 3D thermal convection with variable viscosity: can transient cooling be described by a quasi-static scaling law? Phys. Earth Planet. Inter. 119, 321–336.

Crosby, A.G., McKenzie, D., Sclater, J.G., 2006. The relationship between depth, age and gravity in the oceans. Geophys. J. Int. 166, 553–573.

Crough, S.T., 1978. Thermal origin of mid-plate hot-spot swells. Geophys. J. R. Astron. Soc. 55, 451–470.

Davaille, A., Jaupart, C., 1993. Transient high-Rayleigh-number thermal convection with large viscosity variations. J. Fluid Mech. 253, 141–166.

Davaille, A., Jaupart, C., 1994. Onset of thermal convection in fluids with temperature-dependent viscosity: application to the oceanic mantle. J. Geophys. Res. 99, 19853–19866.

Debayle, E., Sambridge, M., 2004. Inversion of massive surface wave data sets: model construction and resolution assessment. J. Geophys. Res. 109. doi:10.1029/2003JB002652.

Doin, M.P., Fleitout, L., 1996. Thermal evolution of the oceanic lithosphere: an alternative view. Earth Planet. Sci. Lett. 142, 121–136.

Doin, M.P., Fleitout, L., 2000. Flattening of the oceanic topography and geoid: thermal versus dynamic origin. Geophys. J. Int. 143, 582–594.

Dumoulin, C., Doin, M.P., Fleitout, L., 2001. Numerical simulations of the cooling of an oceanic lithosphere above a convective mantle. Phys. Earth Planet. Inter. 125, 45–64.

Dumoulin, C., Doin, M.P., Fleitout, L., Arcay, D., 2005. Onset of small scale instabilities at the base of the lithosphere: scaling laws and role of pre-existing lithospheric structures. Geophys. J. Int. 160, 344–356.

Fjeldskaar, W., 1994. Viscosity and thickness of the asthenosphere detected from the Fennoscandian uplift. Earth Planet. Sci. Lett. 126, 399–410.

Hall, C.E., Gurnis, M., 2005. Strength of fracture zones from their bathymetric and gravitational evolution. J. Geophys. Res. 110. doi:10.1029/2004JB003312.

Haxby, W.F., Weissel, J.K., 1986. Evidence for small-scale convection from seasat altimeter data. J. Geophys. Res. 91, 3507–3520.

Huang, J., Zhong, S., 2005. Sublithospheric small-scale convection and its implications for the residual topography at old ocean basins and the plate model. J. Geophys. Res. 110. doi:10.1029/2004JB003153.

Huang, J., Zhong, S., Van Hunen, J., 2003. Controls on sublithospheric small-scale convection. J. Geophys. Res. 108, 2405–2417.

King, S.D., Anderson, D.L., 1998. Edge-driven convection. Earth Planet. Sci. Lett. 160, 289–296.

Korenaga, J., Jordan, T.H., 2003. Physics of multi-scale convection in the Earth's mantle 1. Onset of sublithospheric convection. J. Geophys. Res. 108. doi:10.1029/2002JB001760.

Maggi, A., Debayle, E., Priestley, K., Barruol, G., 2006. Azimuthal anisotropy of the Pacific region. Earth Planet. Sci. Lett. 250, 53–71.

Marquart, G., 2001. On the geometry of mantle flow beneath drifting lithospheric plates. Geophys. J. Int. 144, 356–372.

Marquart, G., Schmeling, H., Braun, A., 1999. Small-scale instabilities below the cooling oceanic lithosphere. Geophys. J. Int. 138, 655–666.

Montagner, J.P., 2002. Upper mantle low anisotropy channels below the Pacific plate. Earth Planet. Sci. Lett. 202, 263–274.

Morency, C., Doin, M.P., Dumoulin, C., 2005. Three-dimensional numerical simulations of mantle flow beneath mid-ocean ridges. J. Geophys. Res. 110. doi:10.1029/2004JB003454.

Morris, S., Canright, D., 1984. A boundary-layer analysis of Bénard convection in a fluid of strongly temperature-dependent viscosity. Phys. Earth Planet. Inter. 36, 355–373.

Parsons, B., McKenzie, D., 1978. Mantle convection and the thermal structure of the plates. J. Geophys. Res. 83, 4485–4496.

Parsons, B., Sclater, J.G., 1977. An analysis of the variation of ocean floor bathymetry and heat flow with age. J. Geophys. Res. 82, 803–827.

Phipps Morgan, J., Forsyth, D.W., 1988. Three-dimensional flow and temperature perturbations due to a transform offset: effects on oceanic crustal and upper mantle structure. J. Geophys. Res. 93, 2955–2966.

Phipps Morgan, J., Smith, W.H.S., 1992. Flattening of the sea-floor depth–age curve as a response to asthenospheric flow. Nature 359, 524–527.

Raddick, M.J., Parmentier, E.M., Scheirer, D., 2002. Buoyant decompression melting: a possible mechanism for intraplate volcanism. J. Geophys. Res. 107. doi:10.1029/2001jb000617.

Richter, F.M., Parsons, B., 1975. On the interaction of two scales of mantle convection. J. Geophys. Res. 80, 2529–2541.

Ritzwoller, M.H., Shapiro, N.M., Zhong, S., 2004. Cooling history of the Pacific lithosphere. Earth Planet. Sci. Lett. 226, 69–84.

Shen, Y., Forsyth, D.W., 1992. The effects of temperature- and pressure-dependent viscosity on three-dimensional passive flow of the mantle beneath a ridge-transform system. J. Geophys. Res. 97, 19717–19728.

Sigmundsson, F., 1991. Post-glacial rebound and asthenosphere viscosity in Iceland. Geophys. Res. Lett. 18, 1131–1134.

Sleep, N.H., 2002. Local lithospheric relief associated with fracture zones and ponded plume material. Geochem. Geophys. Geosyst. 3. doi:10.1029/2002GC000376.

Solomatov, V.S., Moresi, L.N., 2000. Scaling of time-dependent stagnant lid convection: Application to small-scale convection on Earth and other terrestrial planets. J. Geophys. Res. 105, 21795–21817.

Stein, C.A., Stein, S., 1992. A model for the global variation in oceanic depth and heat flow with lithospheric age. Nature 359, 123–129.

Turcotte, D.L., Oxburgh, E.R., 1967. Finite amplitude convective cells and continental drifts. J. Fluid Mech. 28, 29–42.

van Hunen, J., Zhong, S., 2006. Influence of rheology on realignment of mantle convective structure with plate motion after a plate reorganization. Geochem. Geophys. Geosyst. 7. doi:10.1029/2005GC001209.

van Hunen, J., Huang, J., Zhong, S., 2003. The effect of shearing on the onset and vigor of small-scale convection in a Newtonian rheology. Geophys. Res. Lett. 30. doi:10.1029/2003GL018101.

Zaranek, S.E., Parmentier, E.M., 2004. The onset of convection in fluids with strongly temperature-dependent viscosity cooled from above with implications for planetary lithospheres. Earth Planet. Sci. Lett. 224, 371–386.

Zhong, S., Ritzwoller, M., Shapiro, N., Landuyt, W., Huang, J., Wessel, P., 2007. Bathymetry of the Pacific plate and its implications for thermal evolution of lithosphere and mantle dynamics. J. Geophys. Res. 112. doi:10.1029/2006JB004628.